CrossMark

ORIGINAL PAPER

Observation of the Degradation Characteristics and Scale of Unevenness on Three-dimensional Artificial Rock Joint Surfaces Subjected to Shear

Eun-Soo Hong · Tae-Hyuk Kwon · Ki-Il Song ·
Gye-Chun Cho

Abstract The present study explores the degradation characteristics and scale of unevenness (small-scale roughness) on sheared rock joint surfaces at a low-stress regime. While the degradation characteristics of unevenness and the normal stress are mutually interrelated, an understanding of the degradation patterns of the three-dimensional roughness of rock joints is one of the important components needed to identify asperity failure characteristics and to quantify the role of damaged unevenness in establishing a shear strength model. A series of direct shear tests was performed on three-dimensional artificial rock joint surfaces at different normal stress levels. After shearing, the spatial distributions and statistical parameters of degraded roughness were analysed for the different normal stress levels. The length and area of the degraded zones showed bell-shaped distributions in a logarithmic scale, and the dominant scale (or the most frequently occurring scale) of the damaged asperities (i.e., unevenness) ranged from approximately, 0.5 to 5.0 mm in length and 0.1–10 mm^2 in area. This scale of the damaged unevenness was consistent regardless of the level of normal stress. It was also found that the relative area of damaged unevenness on a given joint area, and thus the contribution of the mechanical asperity failure component to shear strength increased as normal stress increased.

Keywords Roughness degradation · Roughness mobilization · Unevenness scale · Joint shear test · Image analysis

1 Introduction

Shear strength of rock joints is mobilized by two mechanisms: the sliding behavior between joint surfaces and the failure behavior of contacted asperities on a shearing surface (Barton et al. 1985; Swan and Zongqi 1985; Ladanyi and Archambault 1970; Lam and Johnstone 1989). Roughness that contributes to the shear strength of joint rocks is accordingly categorized into two components: a geometrical component related to the sliding behavior and the peak dilation angle, and a mechanical component representing asperity failure (Bandis et al. 1981). The former corresponds to large-scale roughness that causes dilation without failure or degradation, termed waviness; and the later is related to small-scale roughness that tends to be degraded on shearing surfaces, termed unevenness (ISRM 1981).

Normal stress is an important factor in determining the relative contribution of waviness or unevenness to shear strength because normal stress determines the number and area of local contact points of asperities (Teufel and Logan 1978; Logan and Teufel 1986; Xie et al. 1997; Hong et al. 2006a, 2008). For instance, at a low-normal stress level

E.-S. Hong · T.-H. Kwon · G.-C. Cho (✉)
Department of Civil and Environmental Engineering, Korea
Advanced Institute of Science and Technology (KAIST),
Daejeon 305-701, Korea
e-mail: gyechun@kaist.edu

E.-S. Hong
e-mail: neshong@kaist.ac.kr

T.-H. Kwon
e-mail: t.kwon@kaist.ac.kr

K.-I. Song
Department of Civil Engineering, Inha University,
100 Inha-ro, Nam-gu, Incheon 402-751, Korea
e-mail: ksong@inha.ac.kr

Springer

(e.g., $\sigma/JCS < 0.01$), small-scale asperities on a joint surface can contribute to shear strength via a sliding mechanism, increasing peak dilation angle. As the normal stress increases, however, the contribution of the small-scale asperities by sliding is expected to decrease. Instead, mechanical asperity failure becomes significant in mobilizing peak shear strength (Yang et al. 2001; Hong et al. 2006b). Therefore, the relative contribution of waviness or unevenness to shear strength, if the two can be quantified, is not constant but will vary with normal stress. Furthermore, from a strain perspective, it is known that the degradation of unevenness plays a role in mobilizing peak shear strength in a small-strain regime prior to developing peak shear displacement, whereas the dilation caused by waviness and the basic friction angle contribute shear strength regardless of the strain regime. Therefore, quantifying the unevenness on a rock joint surface and identifying the degradation characteristics during shear are important tasks for understanding the roles of unevenness and waviness in mobilizing peak shear strength and for establishing a reliable shear strength model to predict the shear strength of natural rock joints.

Many studies on the shear behavior of rock joint surfaces have been conducted, via empirical methods (Barton 1973; Bandis et al. 1983), introduction of a joint roughness coefficient (Carr and Warriner 1989; Kulatilake et al. 1995; Maerz et al. 1990; Tse and Cruden 1979), and characterization of the failure mechanisms (Lam and Johnstone 1989; Haberfield and Johnston 1994; Yang et al. 2001; Kwon et al. 2010). Micro-scale studies on the three-dimensional degradation of asperities have been performed with experimental approaches (Gentier et al. 2000; Wang and Scholz 1993), theoretical and numerical approaches (Borri-Brunetto et al. 1999; Chiaia 2002; Misra 2002), and by studying 3D joint surface morphology (Belem et al. 2009; Tatone and Grasselli 2013; Mlynarczuk 2010; Jiang et al. 2006). In spite of previous efforts, the degradation characteristics and scale of unevenness remain poorly understood. Yet, they are critical for understanding the asperity failure mechanism and to quantify roughness, and unevenness in particular.

The present study investigated the degradation characteristics and scale of unevenness on artificial rock joint surfaces. Direct shear tests were performed on tensile-fractured surfaces of artificial rock joint specimens at different normal stress levels. The degradation patterns of unevenness were obtained via an image analysis of the sheared surfaces. Spatial distributions and statistical parameters of degradation patterns, such as average, maximum, and minimum scales of the degraded area, were extracted. The effects of normal stress on the degradation characteristics and the scale of unevenness were discussed.

2 Experimental Program

2.1 Preparation of Artificial Joint Rock Specimens

A block of Hamyeol granite, 1.5 m-long, 2.5 m-wide, and 1.5 m-high, was artificially tensile-fractured to create a rough joint surface, and that created tension joint surface was chosen for the present study. Hamyeol granite is one type of Daebo granite, one of the major granites found in the central area of South Korea. It is coarse-grained granite, composed of 29 % quartz, 24 % orthoclase, 25 % plagioclase, and 9 % biotite, and the diameters of these mineral particles were analysed to be 1.0, 3.4, 0.5, and 1.7 mm (average particle size = 0.9 mm), respectively.

Silicon latex (KE-1402, Shin Etsu Co.) was applied on a 1 m × 1 m area of the created rock joint surface to replicate its surface roughness (Hong 2005; Hong et al. 2014). A mixture of the silicon latex and a hardening agent was carefully painted with a brush in a frame of 1 m × 1 m (length × width) on the rock surface and cured for 24 h. Resin has typically been used to replicate fractured surfaces in previous studies (e.g., Gale 1987; Gale et al. 1990; Gentier et al. 1989; Hakami 1995; Hakami and Larsson 1996); however, when the resin is injected, large fractures with small voids may not impregnate with the resin because of the high viscosity. Silicon latex is often used for the replication of complex objects, and we chose to brush the silicon latex liquid to minimize the smoothing of small asperities and the unintended occurrence of air bubbles. When visually inspected, the topology of the joint surface was presumed to be successfully preserved.

Four locations on the surface of the 1 m × 1 m latex replica (i.e., 1st generation replica) were selected to resize the joint specimen for laboratory direct shear tests. Using four different molds with 100 mm × 100 mm × 40 mm dimension, silicon latex was again applied at the selected locations on the 1 m × 1 m replica. Therefore, four 100 mm × 100 mm × 40 mm replica specimens (2nd generation replica), having a three-dimensional roughness, were fabricated and used to reproduce rock joint specimens for laboratory shear tests. High-strength gypsum plaster was used for the reproduction of artificial joint specimens (Hong et al. 2008). Table 1 summarizes the basic properties of the artificial rock joint specimens used in the present study. The upper section (3rd generation replica) was replicated first, and then, the lower section (4th generation replica) was replicated from the upper section. Therefore, a perfectly mated contact condition was achieved. To explore how unevenness degradation affects shear behavior, shear testing of multiple joint sets with identical surface roughness should be conducted at different normal stress levels. It is, however, extremely difficult to obtain multiple sets of natural rock joints with the same (at least, similar)

Table 1 Material properties of the artificial rock joint specimens used

Joint compressive strength (MPa)	Brazilian tensile strength (MPa)	Young's modulus (GPa)	Cohesion (MPa)	Internal friction angle (°)	Basic friction angle (°)	Coefficient of brittleness
40.3	4.0	8.4	9.1	38.1	36.4	10.1

joint roughness morphology. Because of this problem, the artificial rock joint sets used in this study are thought to be an optimal and useful tool to advance our understanding of the effect of normal stress on the degradation characteristics of unevenness in relation to the shear behavior of rough joint surfaces. Note that artificial rock joints made of gypsum plaster can represent sedimentary rock joints (Johnston and Choi 1986; Indraratna and Haque 2000). Thus, the results obtained from this study are applicable to sedimentary rock joints, and may have limitations for crystalline rocks.
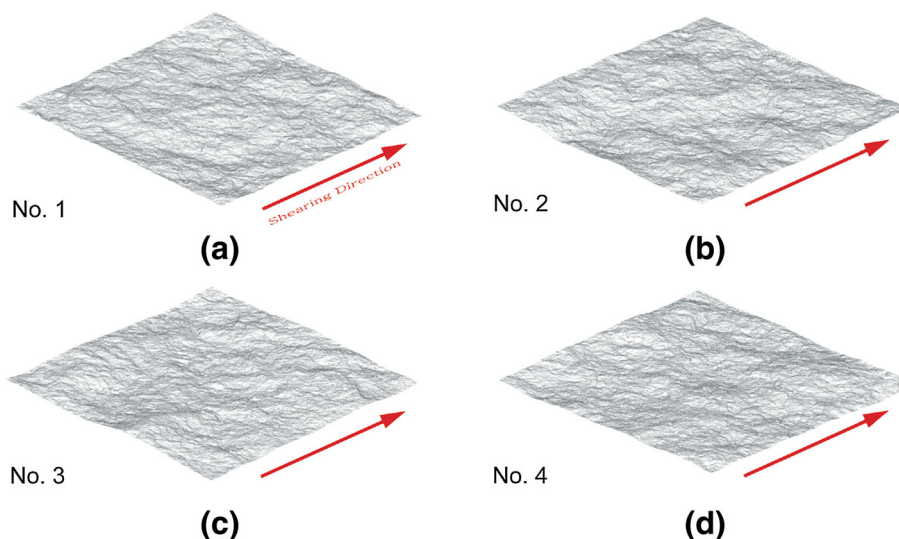
The topology of the surfaces of the four artificial specimens (No. 1, No. 2, No. 3, and No. 4) was obtained using a three-dimensional scanner, as shown in Fig. 1 (Hong et al. 2006a). The surface roughness parameter (R_S), defined as the ratio of the true surface area (A) to the apparent area projected onto the horizontal plane (A_0), was measured to be 1.0869 for Joint No. 1, 1.0876 for Joint No. 2, 1.0889 for Joint No. 3, and 1.0879 for Joint No. 4, respectively (Gokhale and Drury 1990; Gokhale and Underwood 1990). Two-dimensional roughness profiles extracted from each joint surface are presented in Fig. 2. The roughness profiles were extracted parallel to the shearing direction and with a 2-cm space interval; thus five profiles per surface in total. Each joint roughness coefficient (JRC) value was estimated by comparing each profile with the reference profiles suggested by Barton and Choubey (1977). Therefore, a representative JRC value for each surface was calculated by averaging the five JRC values. The average JRC values

were 9.2 for Joint No. 1, 10 for Joint No. 2, 11.6 for Joint No. 3, and 10.8 for Joint No. 4, respectively. In addition, the average inclination angle of asperities (A_i) was obtained in the same manner. The roughness parameters obtained are listed in Table 2, and the order of roughness was No. 3 > No. 4 > No. 2 > No. 1 for R_S, JRC, and A_i.

2.2 Direct Shear Test Results of the Artificial Rock Joint Specimens

A hydraulic shear apparatus (maximum loading capacity: 500 kN) was used for the joint shear tests. The shear tests were performed at five different but constant normal stresses (0.1, 0.25, 0.44, 0.78, 2.25 MPa). This low stress range can represent vertical stress to a depth from 77 to 114 m, assuming the density of overlying layers to be 2000–3000 kg/m^3. This encompasses a range of interest in rock engineering practices at shallow depths, such as rock slopes (Barton 1973). The joint compressive strength (JCS) of the artificial gypsum was measured to be 40.3 MPa; thus, the normal stress normalized by the joint compressive strength (σ/JCS) was 0.0024, 0.0061, 0.011, 0.0195, and 0.056, respectively. The shearing rate was maintained at 0.5 mm/min throughout the experiments, and the shearing was halted when the peak shear stress was confirmed. The vertical displacement and horizontal displacement were monitored using linear variation displacement transducers (LVDTs), while the vertical load and horizontal load were measured using load cells.

Fig. 1 Surfaces of the rock joints used: **a** No. 1, **b** No. 2, **c** No. 3, and **d** No. 4

Fig. 2 Roughness profiles of four joint specimens and the JRC values. The profiles were extracted with a 2-cm interval; H02 is from 1 cm above from the one side edge parallel to the shearing direction, and H06 is from 3 cm above the side edge, and H18 is from 9 cm above the side edge. The JRC values were obtained by comparing each profile with the reference profiles suggested by Barton and Choubey (1977)

The shear test results, shear stress-shear displacement curves and resulting peak shear stresses for different normal stresses are presented in Fig. 3a, b. The stress values are summarized in Table 3. Although the order of the roughness was measured as No. 3 > No. 4 > No. 2 > No. 1, the order of the shear strength was found to be No. 3 > No. 4 > No. 1 > No. 2. The difference between the orders of roughness and shear strength is thought to occur because the roughness parameters only contain the morphological information of average surface roughness, while the shear strength is affected by several factors, including the normal stress, local roughness, or roughest local area of the specimen.

In an attempt to explore the role of asperity degradation in developing peak shear strength, the shearing was halted as soon as the peak shear stress was confirmed to minimize additional shear displacement and to avoid additional degradation while proceeding to a residual state (see Fig. 3a).

However, because of the difficulty in determining the peak shear stress, shear displacements (dh) greater than the peak shear displacements (dh_p) were unavoidable in all tests, as shown in Table 4. The ratio of the shear displacement to the peak shear displacement (dh/dh_p) was approximately, 1.04–2.67, and the peak shear displacement (dh_p) ranged from approximately, 0.3 to 3 mm (Table 4). A general trend was observed in that an increase in normal stress led to an increase in peak shear displacement (Fig. 3c). Typically, a residual state requires more than 10–20 % shear strain; thus, more than 10 to 20-mm shear displacement is required for our specimen size. Compared with these values, the shear displacements in our tests were less than 3.2 mm. Moreover, because the additional shear displacement after peak shear displacement, i.e., dh–dh_p, was less than 1 mm (except for No. 2 under $\sigma_n = 0.10$ MPa; see Table 4), it can be justifiable to assume that this additional shear displacement would not generate significant additional degradation. Consequently, the obtained values presented in Table 5 can be considered more or less representative of the degradation occurring during the process of developing the peak shear strength of the joints. This assumption is also consistent with the previous study by Gentier et al. (2000), where they found that the major degradation of asperities took place prior to or at peak shear displacement during shear.

2.3 Photo Image Analysis

After joint shear testing, a total of 20 sets of joint specimens (i.e., 4 types of surfaces and 5 normal stresses) were collected. One joint set consisted of an upper joint and a lower joint. Because the surfaces of the fabricated rock joints had a pink color, the damaged areas on a sheared surface turned white in color while the undamaged area remained unchanged. Thus, the damaged asperities caused by the shear were visible with the naked eyes and a digital camera, as shown in Fig. 4. Once debris from the damaged asperities was removed with a brush, fine images of the specimen surfaces were taken with a high-resolution digital camera. To minimize distortion in the digital images, the digital camera (Nikon E3500, image resolution 2048 × 1536 dpi) was located above the center of a specimen at a fixed distance from the specimen.

The regions of damaged asperities larger than 0.1 mm, hereafter designated degraded zones, were identified and segmented out from the obtained bitmap images via photo image analysis, as shown in Fig. 4d. The bottom parts of the twenty joint specimens, four types of joints for five different normal stresses, were analysed. Figure 5 shows the segmented images of the degraded zones. Each degraded zone was generated either from a failure of an individual asperity or from abrasive wear of a group of asperities. As expected, it appears that the number of

Table 2 Estimated roughness parameters of the four artificial joint specimens

Roughness parameter	R_S	A_i^a	JRC		
			Comparison with the reference profiles[b]	Back-calculated	
				Low stress at $\sigma/\mathrm{JCS} = 0.0061$	High stress at $\sigma/\mathrm{JCS} = 0.056$
No. 1	1.0869	0.2271	9.2	10.0	12.0
No. 2	1.0876	0.2302	10	7.0	11.3
No. 3	1.0889	0.2430	11.6	15.0	15.4
No. 4	1.0879	0.2326	10.8	13.1	14.3
Mean	1.0878	0.2332	10.4	11.28	13.21
Variance	6.89×10^{-7}	4.75×10^{-5}	1.07	12.40	3.69
Standard dev.	8.30×10^{-4}	6.89×10^{-3}	1.03	3.52	1.92

[a] A_i is the average inclination angle of asperities $A_i = \tan^{-1}\left(\frac{1}{L}\sum_{i=1}^{N-1}|y_{i+1} - y_i|\right)$, where y is the roughness height and N is the number of measurements (Hong et al. 2006b)

[b] The profiles of the joint surfaces were compared with the reference profiles suggested by Barton and Choubey (1977)
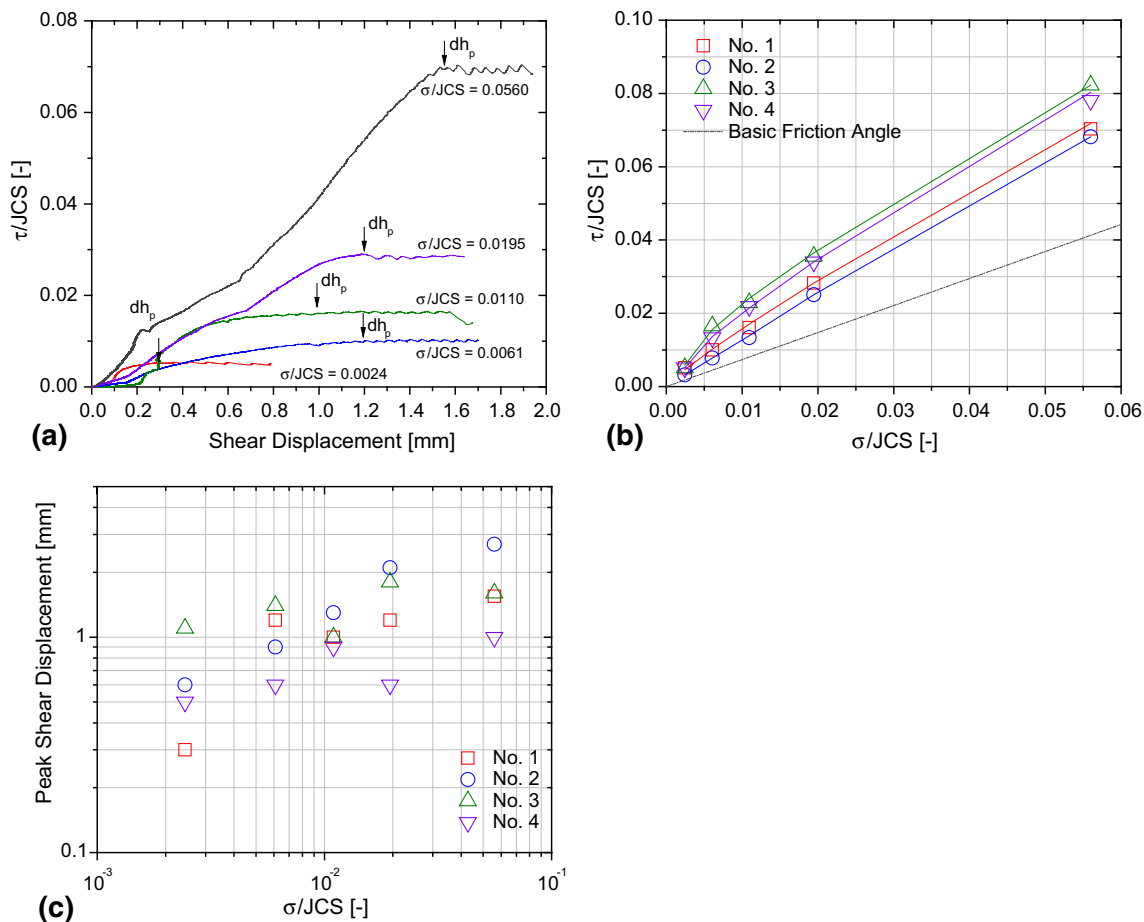

Fig. 3 Results of direct shear tests on the four artificial joint specimens. **a** Shear stress-shear displacement curves of Joint No. 1 in which the peak shear displacement (dh_p) was denoted with *arrows*, **b** peak shear strength (τ/JCS) versus normal stress (σ/JCS), and **c** the changes in the peak shear displacement (dh_p) with normal stress (σ/JCS)

Table 3 Direct shear test results

σ/JCS	Normalized peak shear strength by JCS, τ/JCS			
	No. 1	No. 2	No. 3	No. 4
0.0024	0.0051	0.0032	0.0051	0.0051
0.0061	0.0100	0.0078	0.0165	0.0134
0.0110	0.0161	0.0134	0.0229	0.0219
0.0195	0.0282	0.0251	0.0355	0.0341
0.0560	0.0703	0.0681	0.0823	0.0781

damaged asperities and the total degraded area increased as the normal stress level increased.

Based on the obtained images shown in Fig. 5, various geometric parameters were extracted. These included the number of degraded zones (N); the length of a degraded zone parallel to the shear direction (X_i); the width of a degraded zone perpendicular to the shear direction (Y_i); the average, maximum, and minimum lengths of the degraded zones parallel to the shear direction [Avg(X_i), Max(X_i), and Min(X_i), respectively]; the average, maximum, and minimum widths of the degraded zones perpendicular to the shear direction [Avg(Y_i), Max(Y_i), and Min(Y_i), respectively]; the area of a degraded zone (A_i); the average, maximum, and minimum areas of the degraded zones [Avg(A_i), Max(A_i), and Min(A_i), respectively]; the sum of the degraded area on a specimen (or total degraded area; ΣA_i); the overall area of a joint specimen (A_{joint}); and the ratio of the total degraded area to the overall area of a joint specimen ($\Sigma A_i/A_{joint}$). These values are summarized in Table 5. From these geometric parameters, the degradation characteristics and the scale of asperities were analysed, and their relation to normal stress was discussed.

3 Results and Discussion

3.1 Observations of Degradation Characteristics of Asperities

Based on visual identification of the degradation patterns of asperities, two types of typical asperity degradation characteristics were observed: (1) the individual failure of asperities, and (2) the abrasive wear of asperities (Fig. 4). The failure of asperities was presumably caused by shearing or compression. The abrasive wear indicates a condition where fractions of the solid surface are detached by external forces. Wear can be caused by the adhesion between contact surfaces and abrasion between materials (Bhushan 2002; Rabinowicz 1995). Poon and Sayles (1992) reported that rough or high modulus materials had little adhesion, and the degradation of rock joints was mainly regarded as asperity failure and abrasive wear. It was observed that small and individual asperities failed over a relatively small damaged area (Fig. 4a; the bottom part of the No. 2 specimen sheared at σ/JCS = 0.011). Fragments of failed asperities, sheared off from an undulating joint surface, were found after the completion of shear tests. On the other hand, abrasive wear of asperities was also found over a relatively large area (Fig. 4b, c; the upper part of the No. 1 specimen sheared at σ/JCS = 0.0061 and the bottom part of the No. 2 specimen sheared at σ/JCS = 0.011, respectively). This wear was pronounced in the undulating domains, producing powdery fine particles because of shallow surface degradations.

Figure 5 shows the segmented images of the degraded zones and presents the spatial distributions of the degraded zones for different specimens and different normal stress levels. Presumably, an individual asperity failure or the abrasion of a group of asperities generated each degraded zone. As expected, the number of degraded zones and the total degraded area increased as the normal stress increased. Under a low normal stress condition (σ = 0.1–0.25 MPa or σ/JCS = 0.0024–0.0061), the degraded zones are observed to be spatially scattered. When a medium level of normal stress (σ = 0.44–0.78 MPa or σ/JCS = 0.011–0.0195) was applied, the major degradation occurred at or around the relatively large-scale asperities (undulations or waviness) because of the stress concentration. At the highest normal stress level (σ = 2.25 MPa or σ/JCS = 0.056), the degradation took place over the entire area of the joint specimen, even though joint No. 3 still showed a degradation pattern that was locally concentrated around major undulations.

Table 4 Shear displacements (dh) and peak shear displacements (dh_p) in the shear tests

σ/JCS	No. 1			No. 2			No. 3			No. 4		
	dh (mm)	dh_p (mm)	dh/dh_p(–)	dh (mm)	dh_p (mm)	dh/dh_p (–)	dh (mm)	dh_p (mm)	dh/dh_p (–)	dh (mm)	dh_p (mm)	dh/dh_p (–)
0.0024	0.80	0.30	2.67	1.10	0.60	1.83	1.40	1.10	1.27	1.30	0.50	2.60
0.0061	1.70	1.20	1.42	1.40	0.90	1.56	1.50	1.40	1.07	0.90	0.60	1.50
0.0110	1.70	1.00	1.70	3.20	1.30	2.46	1.10	1.00	1.10	1.10	0.90	1.22
0.0195	1.60	1.20	1.33	2.30	2.10	1.10	2.00	1.80	1.11	0.70	0.60	1.17
0.0560	1.90	1.55	1.23	2.80	2.70	1.04	1.80	1.60	1.13	1.10	1.00	1.10

Table 5 Parameters extracted from the photo image analysis

Joint	σ/JCS (−)	No.	Avg(X_i) (mm)	Min(X_i) (mm)	Max(X_i) (mm)	Avg(Y_i) (mm)	Min(Y_i) (mm)	Max(Y_i) (mm)	Avg(A_i) (mm²)	Min(A_i) (mm²)	Max(A_i) (mm²)	ΣA_i (mm²)	A_{joint} (mm²)	$\Sigma A_i/A_{joint}$ (%)
No. 1	0.0024	75	1.42	0.40	6.10	1.45	0.30	5.60	2.15	0.14	15.68	161.2	12,194	1.32
	0.0061	171	1.09	0.26	3.50	1.14	0.20	4.30	1.28	0.12	8.08	218.1	10,000	2.18
	0.0110	97	1.55	0.50	5.20	1.70	0.30	8.30	2.84	0.15	25.87	275.5	10,000	2.75
	0.0195	149	1.90	0.60	6.60	1.84	0.20	13.20	3.38	0.31	42.75	503.9	10,000	5.04
	0.0560	1167	0.84	0.10	5.70	1.03	0.10	12.40	1.02	0.02	30.16	1194.5	9143	13.06
No. 2	0.0024	27	1.41	0.80	2.50	1.33	0.50	2.80	1.73	0.47	4.81	46.8	10,000	0.47
	0.0061	156	1.05	0.40	3.60	1.01	0.20	6.30	1.06	0.07	8.19	166.1	10,000	1.66
	0.0110	101	2.11	0.60	8.70	1.60	0.40	8.30	3.93	0.24	39.45	397.3	10,000	3.97
	0.0195	221	1.29	0.30	6.30	1.43	0.30	7.20	2.08	0.11	39.21	460.7	10,000	4.61
	0.0560	833	1.30	0.10	11.30	1.37	0.10	11.20	2.28	0.03	105.13	1899.9	10,000	19.00
No. 3	0.0024	48	1.34	0.50	3.00	1.30	0.40	5.90	1.69	0.27	14.03	81.3	10,000	0.81
	0.0061	272	0.74	0.19	2.33	0.84	0.11	3.93	0.66	0.04	8.99	178.7	10,000	1.79
	0.0110	248	1.27	0.30	4.40	1.19	0.30	5.20	1.45	0.10	13.73	359.3	10,000	3.59
	0.0195	127	1.88	0.70	11.10	2.19	0.20	15.10	5.21	0.26	118.50	661.8	10,000	6.62
	0.0560	1215	0.82	0.20	3.00	0.91	0.10	9.70	0.90	0.03	57.20	1090.3	10,000	10.90
No. 4	0.0024	90	1.13	0.20	4.60	1.24	0.20	5.70	1.55	0.10	18.56	139.8	10,000	1.40
	0.0061	109	1.37	0.40	5.20	1.62	0.50	6.10	2.19	0.23	21.31	239.1	10,000	2.39
	0.0110	219	1.28	0.20	4.90	1.30	0.20	6.90	1.96	0.07	27.80	429.4	10,000	4.29
	0.0195	233	1.37	0.40	4.60	1.49	0.20	8.00	2.40	0.07	23.95	558.9	10,000	5.59
	0.0560	564	1.08	0.10	9.00	1.22	0.10	15.60	1.89	0.02	61.96	1063.6	9042	11.76

Fig. 4 Digital images of typical degradation patterns: **a** the *bottom part* of No. 2 specimen sheared at σ/JCS = 0.011, **b** the *upper part* of No. 1 specimen sheared at σ/JCS = 0.0061, **c** the bottom part of No. 2 specimen sheared at σ/JCS = 0.011, and **d** the segmentation of damaged zones on the *bottom part* of No. 3 specimen sheared under σ/JCS = 0.0024
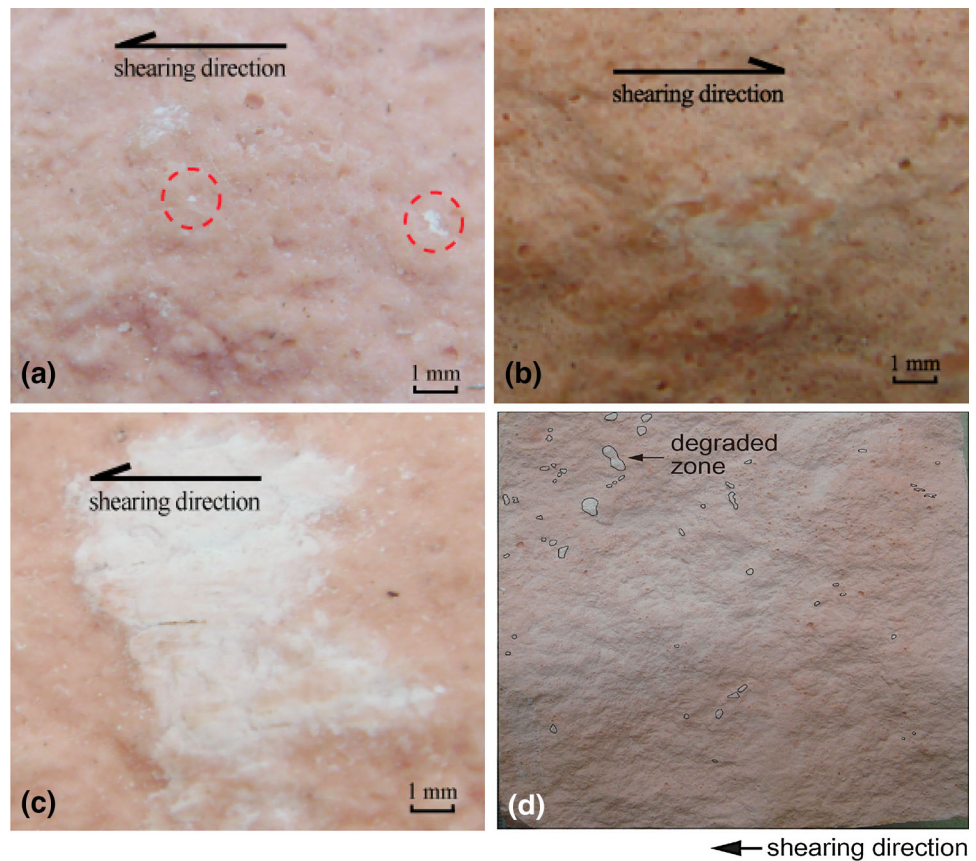
It is a common misconception, typically hypothesized, that the areas degraded at low normal stress would also be degraded at high normal stress. Interestingly, it was found that this was not always the case, as shown in Fig. 5. All asperities in contact at low normal stress should also be in contact at higher stress. However, asperities that are not sheared off under a low normal stress condition can be damaged at higher normal stresses because of better contact and stronger stress concentration. This additional or different asperity failure at a higher stress level changes the dilation behavior of the joints; hence, the contact domains during shear as well. Evidently, several degraded areas identified at low normal stresses (σ = 0.1–0.25 MPa or σ/JCS = 0.0024–0.0061) were not observed at high normal stresses (σ = 0.44–0.78 MPa or σ/JCS = 0.011–0.0195). It is an important implication that not all of the contact domains between joints were degraded during shear at this particular range of normal stress (i.e., σ/JCS = 0.0024–0.0195), and thus, the normal stress level plays a role in determining the spatial distribution of the asperity degradation on a joint surface. This observation is consistent with the results presented by Xie et al. (1997) and Gentier et al. (2000).

3.2 Statistical Distribution of the Scale of the Degraded Zones

Figure 6 presents the histograms of the length of the degraded zone parallel to the shear direction (X_i) plotted in a logarithmic scale. As normal stress increases, the number of degraded areas (N) apparently increases. Bell-shaped distributions are observed in the $\log_{10}$-scale histograms. The degraded zones mostly fall into the lengths of 0.5–5 mm, i.e., the dominant scale of the degraded zones. The histograms of the width of the degraded zone perpendicular to the shear direction (Y_i) show similar results with the histograms of the length of the degraded zone (X_i). It can be found that the length and width of the degraded zones are in the same scale, independent of the shearing direction, as some parameters in Table 5 [e.g., Avg(X_i) and Avg(Y_i)] indicate.

The histograms of the area of the degraded zones (A_i) are shown in Fig. 7. Zones larger than 50 mm^2 are often found. These outliers are hardly observed in low normal stresses (at σ/JCS = 0.0024–0.0061); however, they become frequently observed as the normal stress increases, particularly when the normal stress normalized by the joint compressive strength (σ/JCS) is greater than 0.011. It is
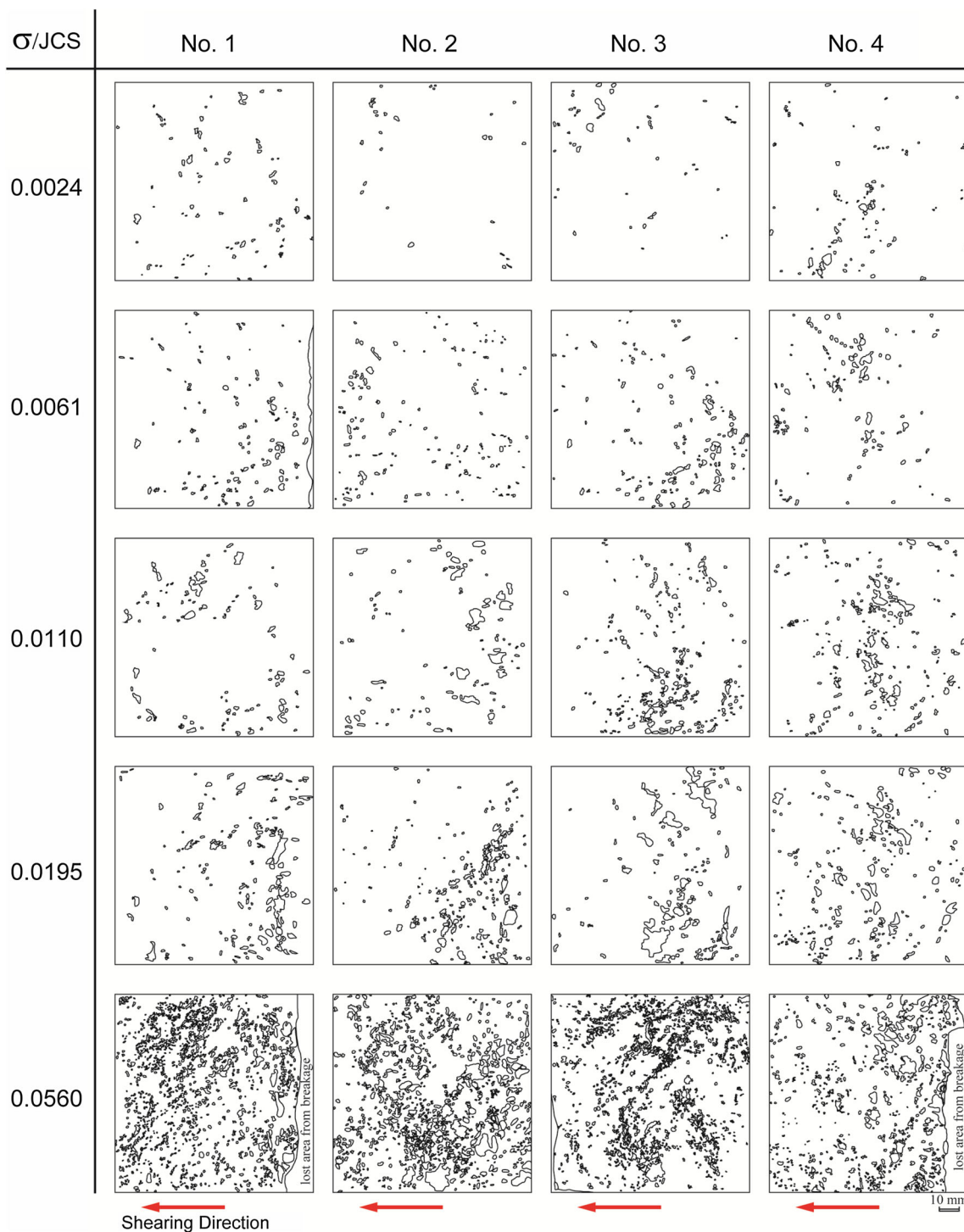
Fig. 5 Segmented images of sheared surfaces for lower joint specimens

presumed that these large degraded zones most likely resulted from the abrasive wear of small-scale asperities (unevenness) with low inclinations. Clear bell-shaped distributions can be observed as well. The degraded zones mostly fall into the area of 0.1–10 mm^2, i.e., the dominant area of the degraded zones. The nominal diameters of the

dominant area, i.e., equivalent diameters where the degraded zones are regarded as a circle, show a range of 0.4–3.4 mm. This is very similar to the results of X_i and Y_i.

As shown in Figs. 6 and 7, the most dominant scale of the damaged unevenness, which impacts mobilized roughness and shear strength, ranges from approximately,
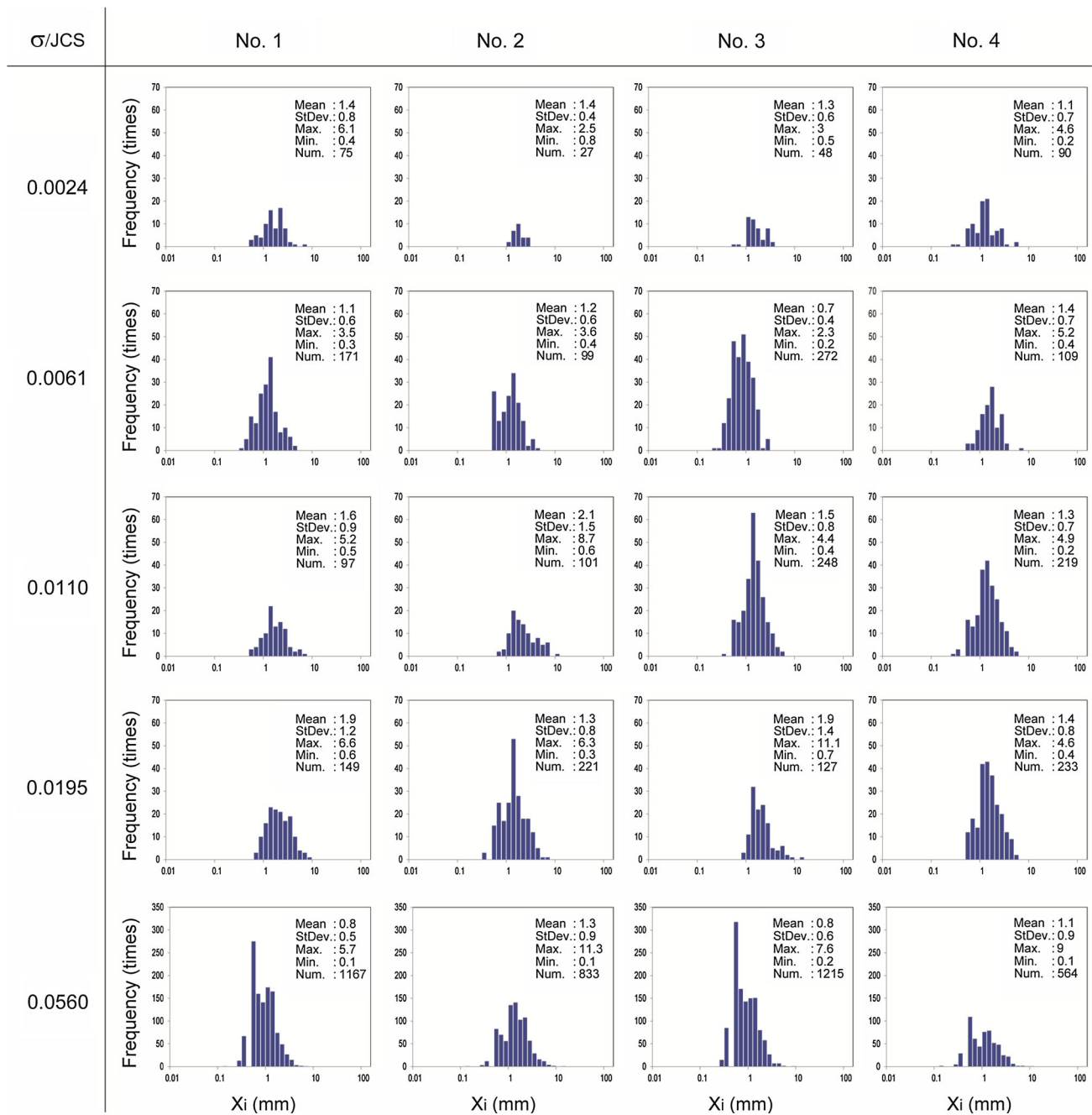
Fig. 6 Histograms of the length of the degraded zone parallel to the shear direction (X_i) in a logarithmic scale

0.5 to 5 mm in size and 0.1–10 mm^2 in area, and this is fairly consistent regardless of normal stress. The normal stress level does not seem to significantly affect the range of scale (length and area) of the damaged unevenness.

3.3 Effect of Normal Stress on Degradation Characteristics

All X_i values measured from a joint specimen are plotted against the normal stress normalized by the joint compressive strength (σ/JCS) in Fig. 8 to see the effect of normal stress on the scale of degraded zones. Although the average length Avg(X_i) or median length of the degraded zone (i.e., the peak of the histograms in Fig. 6) is not related to the normal stress, the plot reveals that the range of X_i becomes wider as the normal stress increases. Moreover, the degradation appears to be more prone to small asperities [i.e., asperities with $X_i <$ Avg(X_i)] than large asperities [i.e., asperities with $X_i >$ Avg(X_i)] as the normal stress increases. For all joint types, the range of X_i is the
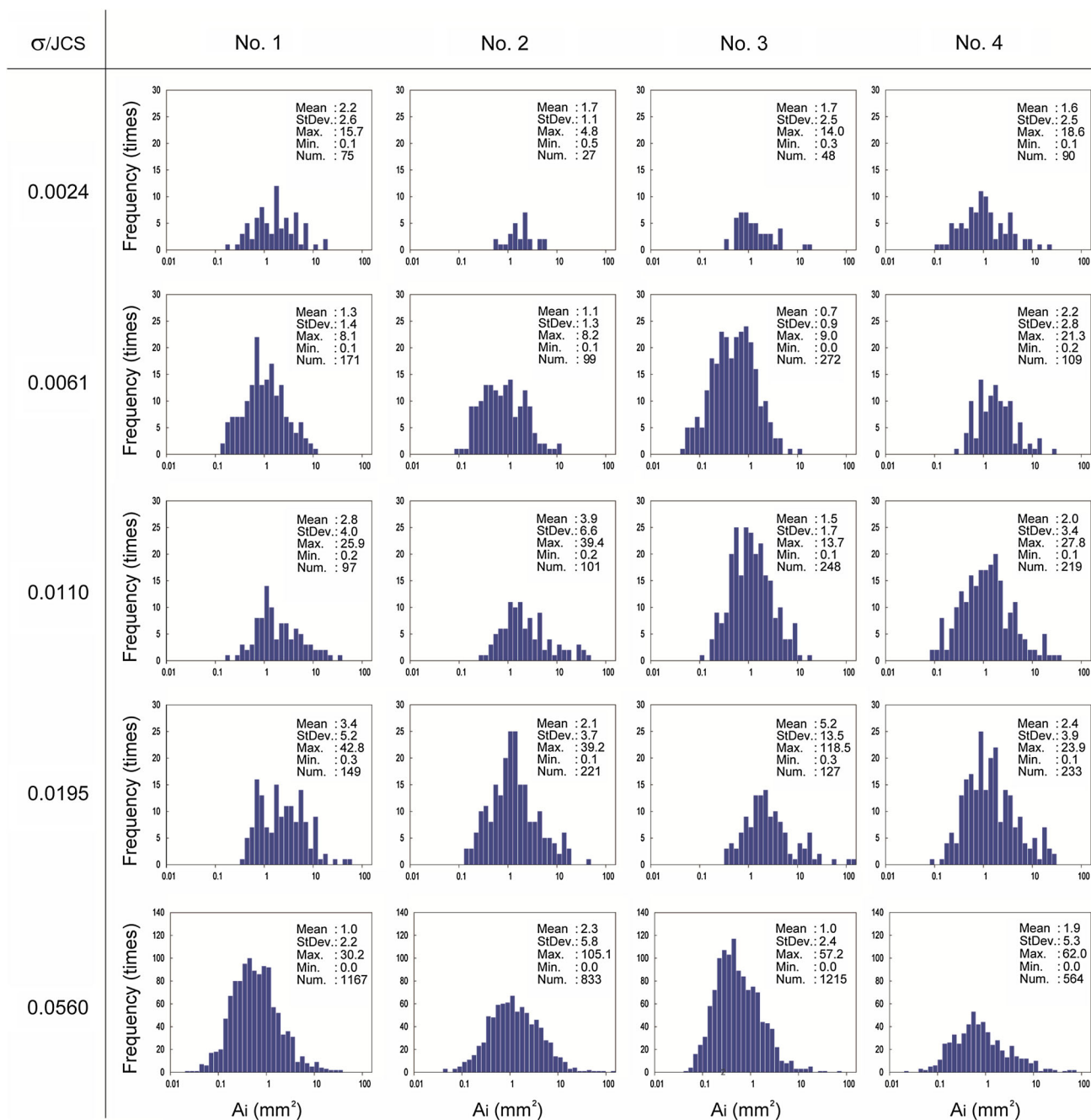
Fig. 7 Histograms of the area of the degraded zone (A_i) in a logarithmic scale

widest at the largest normal stress, and X_i is spread over a range from 0.1 to 11 mm when $\sigma/\text{JCS} = 0.056$ (see Fig. 6).

The ratio of the total degraded area to the overall joint specimen area $\Sigma A_i/A_\text{joint}$ is calculated in a range from 0.4 to 20 %, as shown in Fig. 9a. An increase in the normal stress from $\sigma/\text{JCS} = 0.0024$ to 0.056 led to an increase of $\Sigma A_i/A_\text{joint}$ by more than one order of magnitude. It is found that the ratio of the total degraded area to the joint specimen area ($\Sigma A_i/A_\text{joint}$) and the normal stress (σ/JCS) show a

power-law relationship ($\Sigma A_i/A_\text{joint} = \alpha(\sigma/\text{JCS})^\beta$; Fig. 9a). The number of degraded zones (N) also shows a similar increasing trend with an increase in normal stress but with greater scattering (Fig. 9b). The number of degraded zones (N) is 27–90 at the lowest normal stress ($\sigma/\text{JCS} = 0.0024$) and 564–1215 at the highest normal stress ($\sigma/\text{JCS} = 0.056$), an increase of more than one order of magnitude.

Unevenness, captured by the degraded area, represents the mechanical asperity failure component that contributes
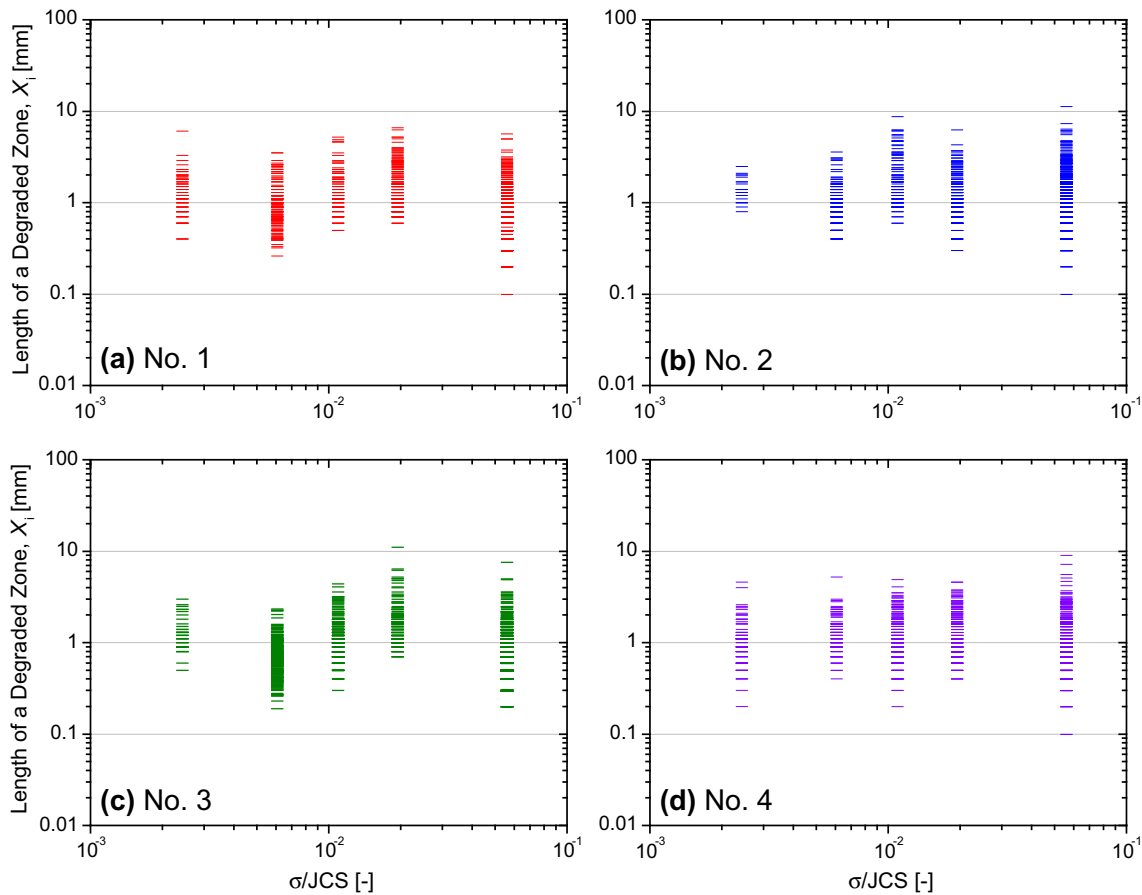
Fig. 8 Length scale of degraded zones (X_i) at different normal stress levels: **a** Joint No. 1, **b** Joint No. 2, **c** Joint No. 3, and **d** Joint No. 4
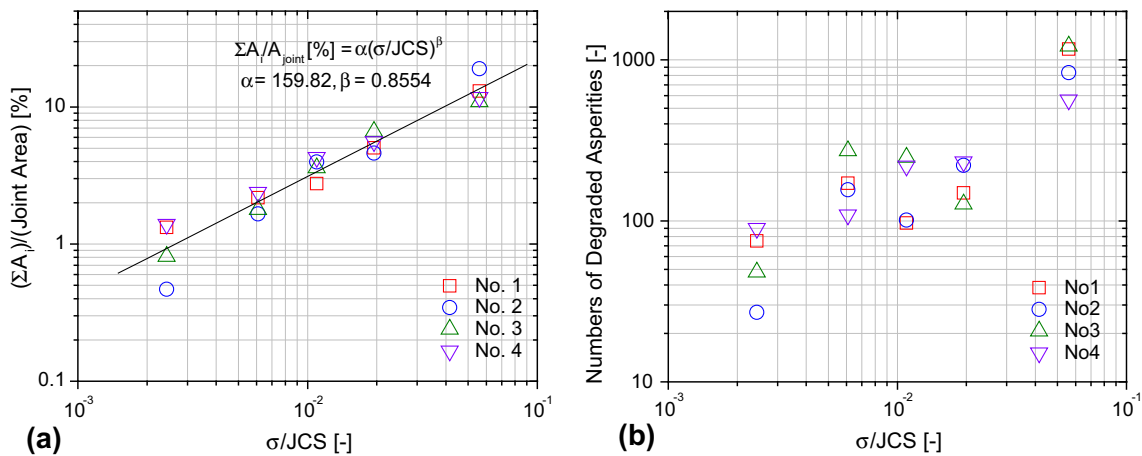

Fig. 9 a Changes in the ratio of the total degraded area to the joint area against the normal stress, and **b** changes in the number of degraded asperities against the normal stress

to shear strength (Bandis et al. 1981; ISRM 1981), Our results provide evidence that the mechanical asperity failure component increases with an increase in normal stress at this particular regime of normal stress (i.e., σ/JCS = 0.0024–0.0195). Furthermore, given that the dominant scale of unevenness stayed fairly consistent regardless of normal stress, the increase in roughness and its contribution to shear strength with the normal stress level is mainly due to the increase in the number of damaged unevenness at this particular range of normal stress (i.e.,

$\sigma/\mathrm{JCS} = 0.0024$–$0.0195$), rather than the size of damaged unevenness.

3.4 The Scale of the Degraded Zones: Average, Maximum, and Minimum Sizes

In Fig. 10, the average, maximum, and minimum lengths of the degraded zones parallel to the shear direction [$\mathrm{Avg}(X_i)$, $\mathrm{Max}(X_i)$, and $\mathrm{Min}(X_i)$, respectively], the average, maximum, and minimum widths of the degraded zones perpendicular to the shear direction [$\mathrm{Avg}(Y_i)$, $\mathrm{Max}(Y_i)$, and $\mathrm{Min}(Y_i)$, respectively), and the average, maximum, and minimum areas of the degraded zones [$\mathrm{Avg}(A_i)$, $\mathrm{Max}(A_i)$, and $\mathrm{Min}(A_i)$, respectively] are plotted against the level of normal stress. It appears that the average lengths, widths, and areas of the degraded zones [$\mathrm{Avg}(X_i)$, $\mathrm{Avg}(Y_i)$, and $\mathrm{Avg}(A_i)$] show a poor correlation with the normal stress, as shown in Fig. 10a. Thus, it is confirmed that the average scales of the degraded zones are hardly affected by normal stress.

However, the maximum length, width, and area of the degraded zones [$\mathrm{Max}(X_i)$, $\mathrm{Max}(Y_i)$, and $\mathrm{Max}(A_i)$] are found to increase with normal stress (Fig. 10b). In contrast, the minimum length, width, and area of the degraded zones [$\mathrm{Min}(X_i)$, $\mathrm{Min}(Y_i)$, and $\mathrm{Min}(A_i)$] show a decreasing trend with an increase in normal stress (Fig. 10c). This is important evidence indicating that shearing under a greater normal stress can damage not only the larger asperities but also the smaller asperities on a rock joint surface.

The average area of the degraded zones $\mathrm{Avg}(A_i)$ has a wider range of values, scattered over one order of magnitude (i.e., 0.5–5 mm^2). The average length and width of the degraded zones $\mathrm{Avg}(X_i)$ and $\mathrm{Avg}(Y_i)$ were in a considerably narrow range and consistently had a value of ~ 1–2 mm, independent of the normal stress (Fig. 10a). Because the area is proportional to the square of the length and width, the areal parameters always present wider ranges than the values of the length and width. The maximum length and width were calculated to be ~ 2–15 mm, while the maximum area was ~ 5–120 mm^2 (see Fig. 10b; Table 5). Last, the minimum length and width were ~ 0.1–0.8 mm, while the minimum area was ~ 0.02–0.5 mm^2 (see Fig. 10b).

It is noted that this minimum length or width of the degraded asperity could be limited mainly by the resolution of the image analysis conducted in the present study. If a
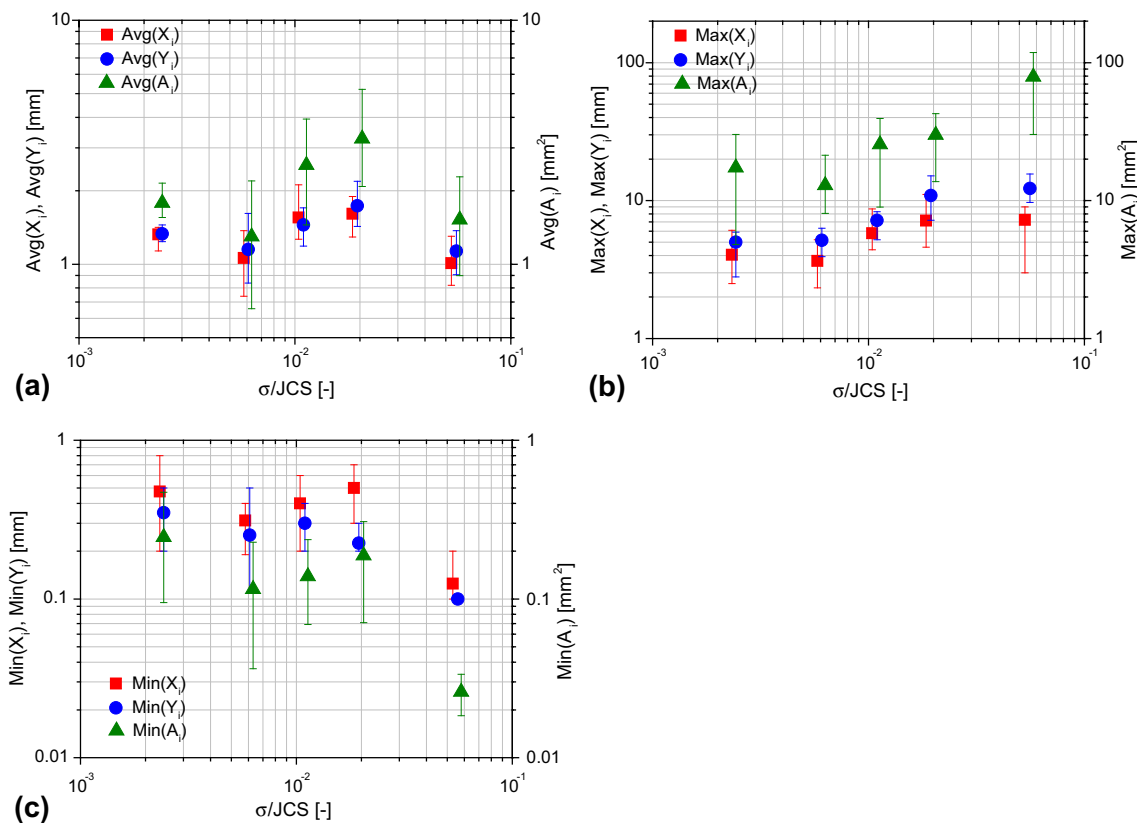

Fig. 10 The effect of normal stress on (**a**) the average length, width, and area of the degraded zones [$\mathrm{Avg}(X_i)$, $\mathrm{Avg}(Y_i)$, and $\mathrm{Avg}(A_i)$]; **b** the maximum length, width, and area of the degraded zones [$\mathrm{Max}(X_i)$, $\mathrm{Max}(Y_i)$, and $\mathrm{Max}(A_i)$]; and **c** the minimum length, width, and area of the degraded zones [$\mathrm{Min}(X_i)$, $\mathrm{Min}(Y_i)$, and $\mathrm{Min}(A_i)$]

higher resolution camera was used to capture a smaller degraded zone, the minimum length, width, and area of the degraded zones under a normal stress of 2.25 MPa (σ/JCS = 0.056) might be lower. Nevertheless, the decreasing trend of the minimum length, width, and area with increasing normal stress is still considered valid.

4 Conclusions

This study explored the degradation characteristics of unevenness (small-scale roughness) during shear, and identified the scale of the damaged unevenness in relation to normal stress at a low-normal stress range. Using laboratory direct shear tests on perfectly mated artificial rock joint specimens with three-dimensional roughness and an image analysis of the sheared joint surfaces, spatial distributions and statistical parameters of the degradation characteristics at different normal stress levels were analysed. Salient findings of this study are as follows:

- Two types of typical degradation characteristics—the individual failure of asperities over a relatively small damaged area and the abrasive wear of asperities over a relatively large area—were readily observed by the naked eye. This wear was pronounced in the undulations, producing powdery fine particles due to shallow and surface degradation.
- The number of the degraded zones and the total degraded area increased as the normal stress increased. Under a low-normal stress condition (σ/JCS = 0.0024–0.0061), the degraded zones were observed to be spatially scattered. When a medium level of normal stress (σ/JCS = 0.011–0.0195) was applied, the major degradation occurred at or around the relatively large-scale asperities (undulations or waviness) because of the stress concentration. At the highest normal stress level (σ/JCS = 0.056), the degradation took place over the entire area of the joint specimen.
- It was found that not all the contact domains between joints were degraded during shear at this particular range of stress (i.e., σ/JCS = 0.0024–0.0195). As a result, several degraded zones identified at a low-normal stress level were not damaged or failed at a higher normal stress level, partially because of different dilation behavior caused by unprecedented asperity failure.
- The histograms of the length of the degraded zone parallel to the shear direction (X_i) and the area of the degraded zones (A_i) showed bell-shaped distributions in a logarithmic scale. The dominant scale and area of the damaged unevenness ranged from $\sim$0.5 to 5.0 and $\sim$0.1 to 10 mm^2. Some degraded areas that were larger

than 50 mm^2 were most likely from abrasive wear of a group of small-scale asperities (unevenness) on undulating domains. It was also found that the length and the width of the degraded zones were in the same scale, independent of the shearing direction.

- The ratio of the total degraded area to the joint specimen area ($\Sigma A_i/A_{joint}$) and the number of degraded zones (N) were correlated to the normal stress (σ/JCS) by a power-law relationship. Therefore, the area of damaged unevenness on a given joint area increased with increasing normal stress because the contribution of roughness to shear strength increased at this particular range of normal stress (i.e., σ/JCS = 0.0024–0.0195). This supports the fact that the contribution of the mechanical asperity failure component to shear strength increases with an increase in normal stress.
- The average scales of the degraded zones (or damaged unevenness) were hardly affected by the normal stress. The maximum size of the degraded zones increased, and the minimum size of the degraded zones decreased with an increase in normal stress, such that the range of damaged unevenness scale became wider. This finding indicates that smaller asperities became more vulnerable to degradation at a higher normal stress.

References

Bandis SC, Lumsden AC, Barton NR (1981) Experimental studies of scale effects on the shear behaviour of rock joints. Int J Rock Mech Min 18(1):1–21

Bandis SC, Lumsden AC, Barton NR (1983) Fundamentals of rock joint deformation. Int J Rock Mech Min 20(6):249–263

Barton NR (1973) Review of a new shear-strength criterion for rock joints. Eng Geol 7:287–332

Barton NR, Choubey V (1977) The shear strength of rock joints in theory and practice. Rock Mech 10:1–54

Barton NR, Bandis SC, Bakhtar K (1985) Strength, deformation and conductivity coupling of rock joints. Int J Rock Mech Min 22:121–140

Belem T, Souley M, Homand F (2009) Method for quantification of wear of sheared joint walls based on surface morphology. Rock Mech Rock Eng 42:883–910

Bhushan B (2002) Introduction to tribology. Wiley, New York

Borri-Brunetto M, Carpinteri A, Chiaia B (1999) Scaling phenomena due to fractal contact in concrete and rock fractures. Int J Fract 95:221–238

Carr JR, Warriner JB (1989) Relationship between the fractal dimension and joint roughness coefficient. Bull Assoc Eng Geol 26:253–264

Chiaia B (2002) On the sliding instabilities at rough surfaces. J Mech Phys Solids 50:895–924

Gale JE (1987) Comparison of coupled fracture deformation and fluid flow models with direct measurements of fracture pore structure and stress-flow properties. In: Proceedings of the 28th U.S. Symposium on Rock Mechanics, A.A. Balkema 1213–1222

Gale J, MacLoad R, LeMessurier P (1990) Site characterization and validation—measurement of flow rate, solute velocities and aperture variation in natural fractures as a function of normal and shear stress, stage 3. Stripa Project Technical Report, 90:11. SKB, Stockholm

Gentier S, Billaux D, van Vliet L (1989) Laboratory testing of the voids of a fracture. Rock Mech Rock Eng 22:149–157

Gentier S, Riss J, Archambault G, Flamand R, Hopkins D (2000) Influence of fracture geometry on shear behavior. Int J Rock Mech Min 37:161–174

Gokhale AM, Drury WJ (1990) A general method for estimation of fracture surface roughness: part II. theoretical aspects. Metall Trans A 21A:1201–1207

Gokhale AM, Underwood EE (1990) A general method for estimation of fracture surface roughness: part I. practical considerations. Metall Trans A 21A:1193–1199

Haberfield CM, Johnston IW (1994) A mechanically-based model for rough rock joints. Int J Rock Mech Min 31(4):279–292

Hakami E (1995) Aperture Distribution of Rock Fractures. Ph. D. thesis, Division of Engineering Geology, Department of Civil and Environmental Engineering, Royal Institute of Technology, Stockholm, Sweden

Hakami E, Larsson E (1996) Aperture measurements and flow experiments on a single natural fracture. Int J Rock Mech Min 33:395–404

Hong ES (2005) Characterization of rock joint roughness based on roughness mobilization characteristics. Ph. D. Thesis, Korea University

Hong ES, Lee IM, Lee JS (2006a) Measurement of rock joint roughness by 3D scanner. Geotech Test J 29(6):482–489

Hong ES, Lee JS, Shin HS, Choi SO, Lee IM (2006b) Characteristics of roughness mobilization. In: Feng Zhou (ed) ISRM International Symposium 2006: 4th Asian Rock Mechanics Symposium—Rock Mechanics in Underground Construction. World Scientific, Singapore

Hong ES, Lee JS, Lee IM (2008) Underestimation of the roughness in rough rock joint. Int J Numer Anal Method Geomech 32:1385–1403

Hong ES, Lee IM, Cho GC, Lee SW (2014) New approach to quantifying rock joint roughness based on roughness mobilization characteristics. KSCE J Civ Eng 18(4):984–991

Indraratna B, Haque A (2000) Shear behaviour of rock joints. Balkema, Rotterdam

ISRM (1981) Suggested method for the quantitative description of discontinuities in rock masse. Rock characterization testing and monitoring. Pergamon press, Oxford, pp 3–52

Jiang Y, Li B, Tanabashi Y (2006) Estimating the relation between surface roughness and mechanical properties of rock joints. Int J Rock Mech Min 43:837–846

Johnston IW, Choi SK (1986) A synthetic soft rock for laboratory model studies. Geotechnique 36(2):251–263

Kulatilake PHSW, Shou G, Huang TH (1995) Spectral-based peak-shear-strength criterion for rock joints. J Geotech Geoenviron 121(11):789–796

Kwon TH, Hong ES, Cho GC (2010) Shear behavior of rectangular-shaped asperities in rock joints. KSCE J Civ Eng 14(3):323–332. doi:10.1007/s12205-010-0323-1

Ladanyi B, Archambault G (1970) Simulation of shear behavior of a jointed rock mass. In: Proceedings of 11th Symposium Rock on Mechanics. Urbana, pp 105–125

Lam TSK, Johnstone IW (1989) Shear behavior of regular triangular concrete/rock joints evaluation. J Geotech Geoenviron 115(5):728–740

Logan JM, Teufel LW (1986) The effect of normal stress on the real area of contact during frictional sliding in rocks. Pageoph 124(3):471–485

Maerz NH, Franklin JA, Bennett CP (1990) Joint roughness measurement using shadow profilometry. Int J Rock Mech Min 27:329–343

Misra A (2002) Effect of asperity damage on shear behavior of single fracture. Eng Fract Mech 69:1997–2014

Młynarczuk M (2010) Description and classification of rock surfaces by means of laser profilometry and mathematical morphology. Int J Rock Mech Min 47:138–149

Poon CY, Sayles RS (1992) The classification of rough surface contacts in relation to tribology. J Phys D Appl Phys 25:A249–A256

Rabinowicz E (1995) Friction and wear of materials, 2nd edn. Wiley, New York

Swan G, Zongqi S (1985) Prediction of shear behaviour of joints using profiles. Rock Mech Rock Eng 18(3):183–212

Tatone BSA, Grasselli G (2013) An investigation of discontinuity roughness scale dependency using high-resolution surface measurements. Rock Mech Rock Eng 46:657–681

Teufel LW, Logan JM (1978) Effect of displacement rate on the real contact and temperatures generated during frictional sliding of Tennessee sandstone. Pageoph 116:840–865

Tse R, Cruden DM (1979) Estimating joint roughness coefficients. Int J Rock Mech Min 16:303–307

Wang W, Scholz CH (1993) Scaling of constitutive parameters of friction for fractal surfaces. Int J Rock Mech Min 30(7):1359–1365

Xie H, Wang J, Xie W (1997) Fractal effects of surface roughness on the mechanical behavior of rock joints. Chaos Soliton Fract 8(2):221–252

Yang ZY, Di CC, Yen KC (2001) The effect of asperity order on the roughness of rock joints. Int J Rock Mech Min 38:745–752